

Bump formation in the runaway electron tail

J. Decker,^{1,*} E. Hirvijoki,² O. Embreus,² Y. Peysson,³ A. Stahl,² I. Pusztai,² and T. Fülöp²

¹*Ecole Polytechnique Fédérale de Lausanne (EPFL), Centre de Recherches
en Physique des Plasmas (CRPP), CH-1015 Lausanne, Switzerland*

²*Department of Applied Physics, Chalmers University of Technology, SE-41296 Gothenburg, Sweden*

³*CEA, IRFM, F-13108 Saint-Paul-lez-Durance, France*

(Dated: August 2, 2018)

Runaway electrons are generated in a magnetized plasma when the parallel electric field exceeds a critical value. For such electrons with energies typically reaching tens of MeV, the Abraham-Lorentz-Dirac (ALD) radiation force, in reaction to the synchrotron emission, is significant and can be the dominant process limiting the electron acceleration. The effect of the ALD-force on runaway electron dynamics in a homogeneous plasma is investigated using the relativistic finite-difference Fokker-Planck codes LUKE [Decker & Peysson, Report EUR-CEA-FC-1736, Euratom-CEA, (2004)] and CODE [Landreman et al, Comp. Phys. Comm. **185**, 847 (2014)]. Under the action of the ALD force, we find that a bump is formed in the tail of the electron distribution function if the electric field is sufficiently large. We also observe that the energy of runaway electrons in the bump increases with the electric field amplitude, while the population increases with the bulk electron temperature. The presence of the bump divides the electron distribution into a runaway beam and a bulk population. This mechanism may give rise to beam-plasma types of instabilities that could in turn pump energy from runaway electrons and alter their confinement.

I. INTRODUCTION

Runaway electrons are typically generated in plasmas in the presence of large electric fields $E > E_c$, where the critical field E_c is defined as [1]

$$E_c = \frac{ne^3 \ln \Lambda}{4\pi\epsilon_0^2 mc^2}, \quad (1)$$

where n is the electron density, m is the electron rest mass, c is the speed of light, e is the elementary charge, and $\ln \Lambda$ is the Coulomb logarithm.

In connection with the sudden cooling in a tokamak disruption, a strong electric field is induced, which leads to the generation of a large number of runaway electrons. In certain cases a significant fraction of the initial toroidal current can be driven by a beam of runaway electrons. The formation of such energetic runaway beams would represent a serious threat for reactor-size machines such as ITER[2]. Consequently, a considerable research effort is currently undertaken to prevent the formation of large runaway beams during tokamak disruptions, or to design a controlled damping scenario for runaway beams if they cannot be avoided [2–6]. The condition $E > E_c$ for runaway electron generation can also be met during the plasma start-up or ramp-down. During the flat-top phase, runaways can appear if the density is sufficiently low in Ohmic plasmas (since $E_c \propto n$), or if an externally applied source of current is suddenly modified.

Experimental measurements show that the maximum runaway electron energy does not increase indefinitely with time but instead reaches a limit in the tens of MeV range [7]. One of the possible mechanisms that could

provide an explanation for this limit is the Abraham-Lorentz-Dirac (ALD) radiation force [8] in reaction to the synchrotron emission due to the particle motion in a magnetic field. For electrons in the MeV range, this force can be significant and contribute to limit the particle acceleration [9]. The synchrotron emission, which carries energy away from the electrons, is also used as a diagnostic tool for the runaway population [10]. The ALD force is characterized by the synchrotron radiation reaction time scale τ_r , given by

$$\tau_r^{-1} = \frac{e^4 B^2}{6\pi\epsilon_0 (mc)^3}, \quad (2)$$

where B is the magnetic field.

In the present paper, the runaway electron dynamics in a homogeneous plasma is investigated using the relativistic finite-difference guiding-center Fokker-Planck codes LUKE [11, 12] and CODE [13, 14]. The electron distribution function evolves under the combined influence of Coulomb collisions, electric field acceleration, and the ALD radiation reaction force. Under a constant parallel electric field (with respect to the magnetic field) $E_{\parallel} > E_c$, the electron distribution never reaches a steady-state in the absence of ALD radiation reaction force. Conversely, it is shown in Sec. III that when the effect of the ALD force is included, the electron distribution evolves towards a steady-state solution. This solution exists even though the synchrotron emission vanishes for electrons with purely parallel motion in a uniform magnetic field. In fact, the expansion of the electron distribution towards higher energies is limited by collisional pitch-angle scattering, which is enhanced by the strong perpendicular anisotropy arising from the combination of electric field acceleration and synchrotron radiation reaction force. This process is found to limit the runaway electron population to energies far below the value for

* joan.decker@epfl.ch

which the contribution from the magnetic field curvature to the ALD radiation reaction force becomes significant [9]. Consequently, it is justified to use the homogeneous plasma limit to study the dynamics of runaway electrons in the core region of tokamaks.

In addition, we show that if the electric field amplitude is sufficiently large, a bump appears in the runaway electron tail of the steady-state distribution function, in accordance with analytical predictions [15]. This bump, which peaks on the parallel axis in momentum space, is entirely located in the runaway region. The steady-state population of electrons in the bump is found to increase with the bulk electron temperature T_e , while their average energy increases with the electric field amplitude E_{\parallel} and decreases with the amplitude of the ALD radiation reaction force, which is proportional to B^2 . For certain parameters, the bump in the electron distribution tail encompasses almost the entire runaway electron population, thus formally dividing the distribution into a bulk population and a runaway beam.

The implementation of the synchrotron reaction force in the kinetic equation is described in Sec. II. The time evolution of the electron distribution calculated by the Fokker-Planck modelling code LUKE is presented in Sec. III. The properties of the steady-state distribution function and the mechanism leading to the formation of a bump are described in Sec. IV, where a comparison between the codes LUKE and CODE is also presented. The bump is characterized in Sec. V as a function of the electric field amplitude, ALD radiation reaction, bulk electron temperature, and ion effective charge. Implications of the ALD radiation reaction force and bump-in-tail formation are discussed in the Conclusions, Sec. VI.

II. SYNCHROTRON REACTION FORCE IN THE KINETIC EQUATION

A. Kinetic equation for charged particles in a magnetized plasma

The kinetic equation for species a with charge q and mass m is given by

$$\frac{\partial f_a}{\partial t} + \frac{\partial}{\partial \mathbf{x}} \cdot (\dot{\mathbf{x}} f_a) + \frac{\partial}{\partial \mathbf{p}} \cdot (\dot{\mathbf{p}} f_a) = C[f_a, f_b], \quad (3)$$

where $C[f_a, f_b]$ is the collision operator between particle species a and b (including intra-species collisions) and $(\dot{\mathbf{x}}, \dot{\mathbf{p}})$ are the equations of motion associated with phase-space coordinates (\mathbf{x}, \mathbf{p}) . Here \mathbf{x} is the particle position and $\mathbf{p} = \gamma m \mathbf{v}$ is the particle momentum, with $\gamma = 1/\sqrt{1 - v^2/c^2} = \sqrt{1 + p^2/(mc)^2}$ the relativistic factor. In the Fokker-Planck limit, the Coulomb collision operator is given by

$$C_{\text{FP}}[f_a, f_b] = -\frac{\partial}{\partial \mathbf{p}} \cdot \left(\mathbf{K}_{\text{FP}ab}[f_b] f_a - \mathbb{D}_{\text{FP}ab}[f_b] \cdot \frac{\partial f_a}{\partial \mathbf{p}} \right), \quad (4)$$

where $\mathbf{K}_{ab}[f_b]$ is the collisional friction vector and $\mathbb{D}_{ab}[f_b]$ is the collisional diffusion tensor. The relativistic Braams-Karney collision operator is used in this paper [16, 17].

So-called *knock-on* collisions represent a $1/\ln \Lambda$ correction to the collision operators. However, when the runaway population becomes significant, these collisions can play an important role as they give rise to an avalanche effect that can significantly increase the runaway growth rate. This secondary runaway generation is neglected in the present work, which is restricted to situations where the runaway population is sufficiently small for secondary electron generation to be negligible. However, it is possible that the ALD radiation reaction force has a significant effect on the secondary runaway generation. Such considerations will be the subject of future work.

The equations of motion combine the Hamiltonian motion from the electric and magnetic fields \mathbf{E} and \mathbf{B} , and the effect of the ALD radiation reaction \mathbf{F}_{ALD} :

$$\dot{\mathbf{x}} = \mathbf{v}, \quad (5)$$

$$\dot{\mathbf{p}} = q(\mathbf{E} + \mathbf{v} \times \mathbf{B}) + \mathbf{F}_{\text{ALD}} \equiv \mathbf{F}_E + \mathbf{F}_m + \mathbf{F}_{\text{ALD}}. \quad (6)$$

The Abraham-Lorentz-Dirac force describes momentum loss in reaction to the synchrotron radiation, and takes the form [8]

$$\mathbf{F}_{\text{ALD}} = \frac{q^2 \gamma^2}{6\pi \epsilon_0 c^3} \left[\ddot{\mathbf{v}} + \frac{3\gamma^2}{c^2} (\mathbf{v} \cdot \dot{\mathbf{v}}) \dot{\mathbf{v}} + \frac{\gamma^2}{c^2} \left(\mathbf{v} \cdot \ddot{\mathbf{v}} + \frac{3\gamma^2}{c^2} (\mathbf{v} \cdot \dot{\mathbf{v}})^2 \right) \mathbf{v} \right]. \quad (7)$$

In magnetically confined fusion plasmas, the magnetic force $\mathbf{F}_m = q \mathbf{v} \times \mathbf{B}$ characterized by the Larmor frequency $\omega_c = qB/m$ typically dominates both the electric force $\mathbf{F}_E = q\mathbf{E}$ and the radiation reaction force \mathbf{F}_{ALD} such that $\mathbf{v} \cdot \dot{\mathbf{v}} \simeq 0$. In a uniform constant magnetic field, the ALD force (7) thus reduces to

$$\mathbf{F}_{\text{ALD}} \simeq -\frac{m}{\tau_r} \left[\mathbf{v}_{\perp} + \frac{\gamma^2 v_{\perp}^2}{c^2} \mathbf{v} \right], \quad (8)$$

where $\mathbf{v}_{\perp} = (\mathbf{I} - \hat{\mathbf{b}}\hat{\mathbf{b}}) \cdot \mathbf{v}$ is the perpendicular velocity with norm $v_{\perp} = \|\mathbf{v}_{\perp}\|$ and $\hat{\mathbf{b}} = \mathbf{B}/B$ is the magnetic field unit vector.

B. Guiding-center transformation

In fusion plasmas, the gyroperiod is short compared to the time scale associated with collisions, the ALD radiation reaction force, and the electric field acceleration. Based on this time-scale separation, the kinetic equation is reduced by eliminating the gyromotion in Eq. (3) using Lie-transform perturbation methods [18, 19]. The transformation of the dissipative ALD force uses the Lie-transform for non-Hamiltonian dynamics, which has been

recently derived in Ref. [20]. In a uniform plasma, the re-sulting guiding-center distribution function for electrons evolves in the 2-D gyro-angle independent momentum space (p, ξ) as

$$\frac{\partial f}{\partial t} + \nabla_{p,\xi} \cdot \mathbf{S}_{p,\xi}[f] = I_{\text{FP}}[f], \quad (9)$$

where p is the guiding-center momentum and $\xi = p_{\parallel}/p$ is the pitch-angle cosine. Components of the guiding-center momentum-space flux

$$\mathbf{S}_{p,\xi}[f] = (\mathbf{K}_{\text{FP}} + \mathbf{K}_{\text{E}} + \mathbf{K}_{\text{ALD}})f - \mathbb{D}_{\text{FP}} \cdot \nabla_{p,\xi} f \quad (10)$$

include convective contributions from collisional drag \mathbf{K}_{FP} , electric field acceleration \mathbf{K}_{E} , and the radiation reaction force \mathbf{K}_{ALD} , and a collisional diffusion tensor \mathbb{D}_{FP} . The integral part of the guiding-center collisional operator is denoted $I_{\text{FP}}[f]$. It describes the evolution of the bulk population due to collision with fast electrons. When momentum conservation of the electron-electron collision operator is essential - as for the calculation of electron-driven current - the term $I_{\text{FP}}[f]$ must be included [21]. It is generally truncated at the first order in Legendre expansion. The truncation ensures momentum conservation but allows energy dissipation such that it is not necessary to model energy transport to reach a steady-state solution. In the present paper, the term is set to zero unless otherwise specified. Omitting $I_{\text{FP}}[f]$ makes it possible to use the stream function to interpret the steady-state fluxes in momentum space, as seen in Sec. IV A. It also allows a comparison between the codes LUKE and CODE, since the integral part of the collision operator is not yet included in CODE. This benchmark is presented in Sec. IV D, where it is also shown that the effect of $I_{\text{FP}}[f]$ on the tail of the electron distribution can be neglected.

Writing out the momentum space divergence operator explicitly, the kinetic equation (9) becomes

$$\frac{\partial f}{\partial t} + \frac{1}{p^2} \frac{\partial}{\partial p} (p^2 S_p) - \frac{1}{p} \frac{\partial}{\partial \xi} (\sqrt{1-\xi^2} S_{\xi}) = 0, \quad (11)$$

where the guiding-center momentum space flux components are

$$\begin{aligned} S_p &= -D_{pp,\text{FP}} \frac{\partial f}{\partial p} + (K_{p,\text{FP}} + K_{p,\text{E}} + K_{p,\text{ALD}})f, \\ S_{\xi} &= \sqrt{1-\xi^2} D_{\xi\xi,\text{FP}} \frac{\partial f}{\partial \xi} + (K_{\xi,\text{E}} + K_{\xi,\text{ALD}})f. \end{aligned} \quad (12)$$

The terms contributing to these fluxes are the convection and diffusion coefficients associated with the Fokker-Planck collision operator (which are independent of ξ for isotropic field particle distributions [16, 17])

$$D_{pp,\text{FP}} = A_{\text{FP}}(p), \quad (13)$$

$$K_{p,\text{FP}} = -F_{\text{FP}}(p), \quad (14)$$

$$D_{\xi\xi,\text{FP}} = \frac{B_{\text{FP}}(p)}{p}, \quad (15)$$

the electric field acceleration

$$K_{p,\text{E}} = \xi E_{\parallel}, \quad (16)$$

$$K_{\xi,\text{E}} = -\sqrt{1-\xi^2} E_{\parallel}, \quad (17)$$

and the synchrotron reaction force

$$K_{p,\text{ALD}} = -\sigma_r \gamma p (1 - \xi^2), \quad (18)$$

$$K_{\xi,\text{ALD}} = -\sigma_r \frac{p \xi \sqrt{1-\xi^2}}{\gamma}. \quad (19)$$

In Eqs. (11-19), time is normalized to the collision time for relativistic electrons,

$$\tau_c = \frac{4\pi\epsilon_0^2 m^2 c^3}{e^4 n \ln \Lambda}, \quad (20)$$

momentum p is given in units of mc , the parallel electric field E_{\parallel} is normalized to the critical field E_c , and $\sigma_r \equiv \tau_c/\tau_r$ measures the relative strength (compared to collisional forces) of the ALD radiation reaction force

$$\sigma_r = \frac{2}{3} \frac{1}{\ln \Lambda} \frac{\omega_c^2}{\omega_p^2}, \quad (21)$$

where ω_p is the electron plasma frequency defined by $\omega_p^2 = e^2 n / (\epsilon_0 m)$. The collisional diffusion coefficients $A_{\text{FP}}(p)$ and $B_{\text{FP}}(p)$ are normalized to $(mc)^2/\tau_c$ while the friction coefficient $F_{\text{FP}}(p)$ is normalized to mc/τ_c .

An explicit form of the momentum-space fluxes (12) is thus

$$\begin{aligned} S_p &= -A_{\text{FP}}(p) \frac{\partial f}{\partial p} + [\xi E_{\parallel} - F_{\text{FP}}(p) - \sigma_r \gamma p (1 - \xi^2)] f, \\ S_{\xi} &= \sqrt{1-\xi^2} \left(\frac{B_{\text{FP}}(p)}{p} \frac{\partial f}{\partial \xi} - E_{\parallel} - \sigma_r \gamma^{-1} p \xi \right) f. \end{aligned} \quad (22)$$

We assume cold and infinitely massive ions, so that the normalized collision coefficients A_{FP} , F_{FP} and B_{FP} only depend on T_e and Z_{eff} [17]. Collisions with ions only enter the pitch-angle scattering term $B_{\text{FP}}(p) = B_{\text{FP},e}(p) + Z_{\text{eff}}/(2v)$, while $A_{\text{FP}}(p) = \beta^2 F_{\text{FP}}(p)/v$, where the normalized electron temperature is defined as $\beta^2 \equiv k_B T_e / (mc^2)$. To summarize, the normalized equation (22) depends on the following independent parameters only: the parallel electric field E_{\parallel} , the normalized ALD frequency σ_r , the electron temperature T_e , and the effective charge Z_{eff} .

III. EVOLUTION OF THE ELECTRON DISTRIBUTION FUNCTION

A. Force balance and runaway region

Some preliminary insight into runaway electron dynamics can be extracted from the force balance, $K_p \equiv K_{p,\text{FP}} + K_{p,\text{E}} + K_{p,\text{ALD}} = 0$, which can be expressed as

$$\xi E_{\parallel} - F_{\text{FP}}(p) - \sigma_r \gamma p (1 - \xi^2) = 0. \quad (23)$$

In the high velocity limit (see Appendix B) and in the absence of the ALD force, the force balance yields

$$p^2 = \frac{1}{\xi E_{\parallel} - 1}. \quad (24)$$

For particles with purely parallel momentum, this condition determines the critical momentum $p_c \equiv (E_{\parallel} - 1)^{-1/2}$ above which electrons are continuously accelerated. For particles with very large momentum $p \gg 1$, the condition (24) provides an asymptotic value $\xi_c = E_{\parallel}^{-1}$, such that $K_p > 0$ for particles with $\xi > \xi_c$.

In this paper, the runaway region is defined as the region where the momentum force balance is positive, i.e. $K_p > 0$. Electrons located within this region are considered runaway electrons. In the absence of the ALD force, this definition corresponds to the usual idea of a runaway electron, as the probability for an electron to be continuously accelerated if it enters the region where $K_{p,FP} + K_{p,E} > 0$ is very high. The momentum space described by finite-difference Fokker-Planck codes is a limited domain by nature with a high-energy boundary defined by a maximum momentum p_{\max} . A proper description of the runaway dynamics clearly requires $p_{\max} \gg p_c$. Then, we must distinguish between electrons located in the $K_{p,FP} + K_{p,E} > 0$ region within the code simulation domain $p < p_{\max}$, *internal runaways*, and electrons having left the simulation domain, *external runaways*. The total runaway population n_r consists of both internal and external runaways, the latter being counted in the simulation, albeit without following their momentum space characteristics.

When the ALD force is included, and for relativistic electrons with $p_{\parallel} \gg 1$ and $p_{\parallel} \gg p_{\perp}$, the force balance (23) is approximately given by

$$E_{\parallel} - 1 - \sigma_r p_{\perp}^2 = 0 \quad (25)$$

and yields a condition on the perpendicular momentum ($p_{\perp} \equiv p\sqrt{1 - \xi^2}$)

$$p_{\perp 0}^2 = \frac{E_{\parallel} - 1}{\sigma_r}. \quad (26)$$

The momentum space in the far tail of the distribution is separated into the runaway region $p_{\perp} < p_{\perp 0}$ where the electric force dominates over the ALD force and the collisional drag such that the net force is positive, and a region $p_{\perp} > p_{\perp 0}$ where the ALD force and collisional drag dominate the electric force such that the net force is negative.

As the calculations in the next sections will show, in the presence of an ALD force, the probability for electrons with $K_p > 0$ to escape the runaway region at some point is high. Therefore, the concept of a runaway electron in this case is more an extension of the usual definition than a true characteristic. We will also see that electrons labelled as runaways can be entirely kept within the simulation domain such that there are no external runaways.

B. The Fokker-Planck code LUKE

The Fokker-Planck equation is solved numerically by the relativistic guiding-center Fokker-Planck code LUKE. Equation (9) is discretized in momentum space (p, ξ) using a 2-D finite-difference scheme with non-uniform grids and a 9-point differentiation procedure. A total of 1200 points are used for the p grid, with 140 grid points describing the $0 < p < 3$ region with a constant grid step, and 1060 grid points describing the $3 < p < p_{\max} = 200$ region using increasing grid steps with cubic dependence. A total of 166 points are used for the ξ grid, with a decreasing step size towards $\xi = \pm 1$ for increased resolution near the p_{\parallel} axis. The code LUKE has been benchmarked for the usual runaway problem [11]. A benchmark including the ALD radiation reaction force is conducted against the Fokker-Planck solver CODE and presented in Sec. IV D.

The linearization of the electron-electron collision operator implies that the calculation is valid only as long as the electron distribution is not too distorted from the original Maxwellian, which in practice implies that the runaway fraction n_r/n does not exceed a few percent.

C. Time evolution of the distribution function

The electron distribution evolves from an initial relativistic Maxwellian distribution, which is also the steady-state solution of Eq. (11) for $E_{\parallel} = 0$ and $\sigma_r = 0$. A constant electric field $E_{\parallel} = 3$ is applied, the effective charge is $Z_{\text{eff}} = 1$, the temperature is $\beta = 0.1$ ($T_e = 5.11$ keV), and the ratio B^2/n is adjusted such that $\sigma_r = 0.6$, which corresponds to typical low-density conditions in tokamak plasmas (i.e. $n = 10^{19} \text{ m}^{-3}$ and $B = 4$ T in the Tore-Supra tokamak). The evolution of the electron distribution function in the parallel direction ($\xi = 1$) is shown in Fig. 1.

In the absence of the ALD force, a runaway tail progressively extends to the edge of the simulation box (Fig. 1(a)). The electron distribution does not converge to a steady-state. The runaway rate reaches an asymptotic value (Fig. 1(e)), and the fraction of runaway electrons increases continuously (Fig. 1(c)). At first, the runaway rate is related to an increase in the internal runaway electron population. Once the runaway tail reaches the edge of the simulation domain (for $t \sim 200$), the runaway rate is related to the population leaving the simulation box and becoming external runaways. Note that, strictly speaking, the linearized collision operator is no longer valid for $t/\tau_c > 10^5$ as the fraction of runaway electrons becomes of order unity. Nevertheless, the evolution is continued to illustrate the absence of a steady-state solution. In summary, the distribution function (Fig. 1(a)) evolves towards an asymptotic solution with the bulk population depleting at a constant rate.

In the presence of the ALD force, however, we find that the distribution evolves towards a steady-state solu-

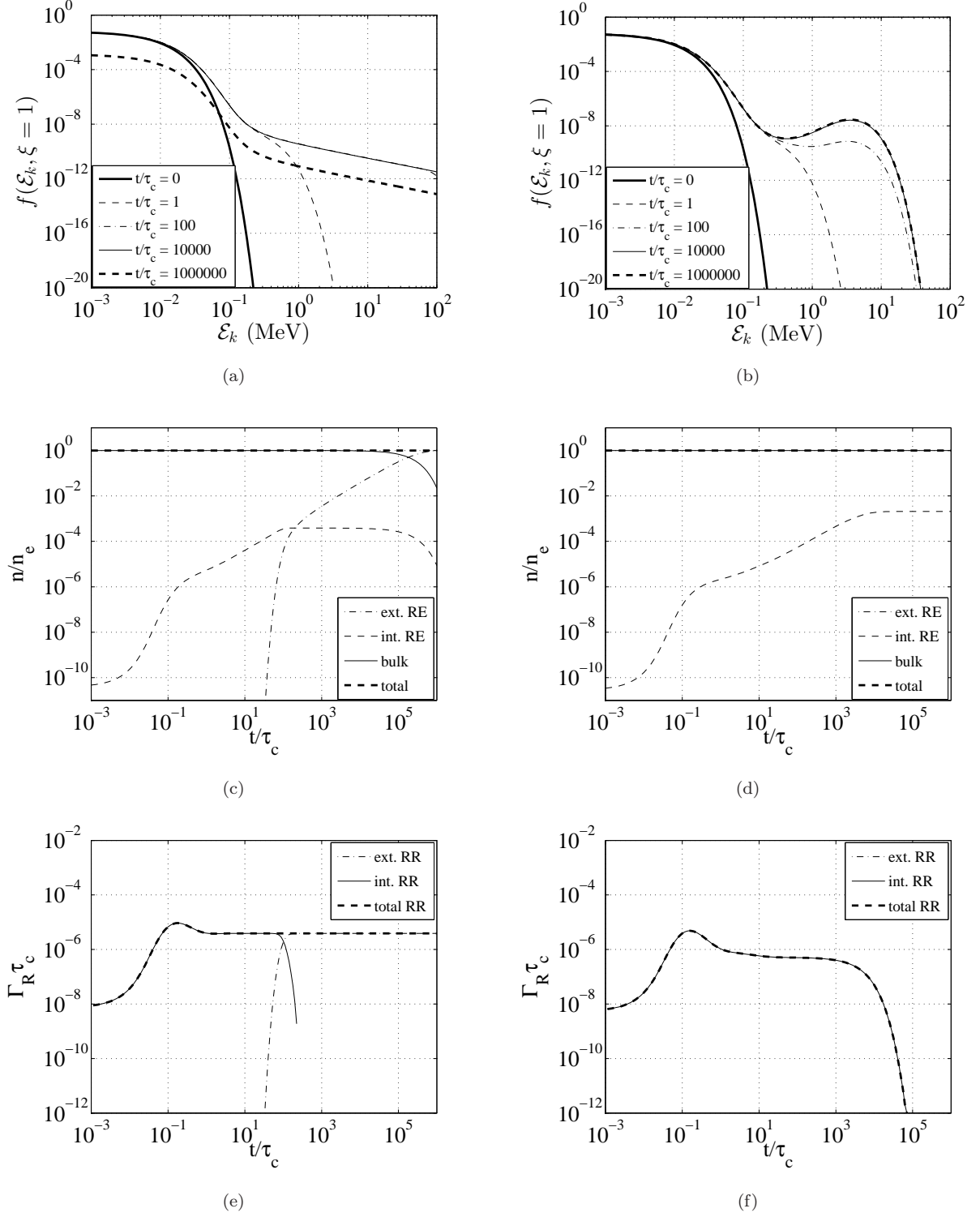


FIG. 1. Graphs (a) and (b) represent the evolution of the electron distribution function in the parallel direction ($\xi = 1$) as a function of the electron kinetic energy \mathcal{E}_k ; graphs (c) and (d) show the fraction of runaway electrons (RE) inside and outside the simulation domain, and graphs (e) and (f) the corresponding runaway rates. The parameters are $E_{\parallel} = 3$, $Z_{\text{eff}} = 1$, $\beta = 0.1$, and $\sigma_r = 0.6$. The ALD force contribution is neglected in graphs (a,c,e), whereas it is included in graphs (b,d,f).

tion (Fig. 1(b)) as the runaway rate vanishes (Fig. 1(f)). No electron leaves the simulation box, and the population of internal runaways reaches an asymptotic value $n_r/n = 0.002$ (Fig. 1(d)). In addition, we can observe the formation of a region with positive gradient in parallel momentum, which appears as a high-energy bump in the tail of the distribution function (Fig. 1(b)). Properties of the time-asymptotic electron distribution function are examined in the next section.

IV. STEADY-STATE SOLUTION AND BUMP FORMATION

A. Steady-state solution

If a steady-state solution exists, it satisfies the equation $\nabla_{p,\xi} \cdot \mathbf{S}_{p,\xi} = 0$. Given the axisymmetry of the momentum space, the divergence-free steady-state fluxes can be expressed as

$$\mathbf{S}_{p,\xi} = \nabla_{p,\xi} \times \left[\frac{A(p,\xi)}{2\pi p \sqrt{1-\xi^2}} \hat{\boldsymbol{\varphi}} \right], \quad (27)$$

where $A(p,\xi)$ is called the stream function. Since $\mathbf{S}_{p,\xi} \cdot \nabla_{p,\xi} A = 0$, contours of $A(p,\xi)$ indicate the direction of the momentum-space fluxes, or streamlines. The total flux of electrons between two contours is given by the corresponding difference in the value of $A(p,\xi)$, such that narrowing contours indicate regions of stronger flux. The stream function thus provides a very informative graphical representation of the steady-state fluxes in momentum space. While no steady-state solution to the runaway problem exists in the absence of ALD force, it is possible to artificially obtain a steady-state distribution function by adding a source term at $p = 0$, which compensates exactly for the external runaway rate. Whereas adding cold electrons does not change the runaway rate or the shape of the distribution function in the tail, it enables us to interpret the stream function as a representation of the steady-state fluxes.

The 2D representation of the steady-state solution corresponding to the simulation parameters from Section III C is presented in Fig. 2. The distribution function is shown in Figs. 2(a) and 2(b) for the case without and with ALD force, respectively. The dashed line delimits the runaway region where $K_p > 0$. The corresponding contours of the stream function $A(p,\xi)$ are drawn in Figs. 2(c) and 2(d).

In the absence of the ALD force, the runaway population peaks near the p_{\parallel} axis but extends quite far in the perpendicular direction into the runaway region, as seen in Fig. 2(a). The open streamlines represented by the contours of the stream function in Fig. 2(c) show that electrons located in the runaway region are indefinitely accelerated and eventually escape the simulation domain.

In the presence of the ALD force, the runaway region consists of a narrow band along the p_{\parallel} axis delimited by

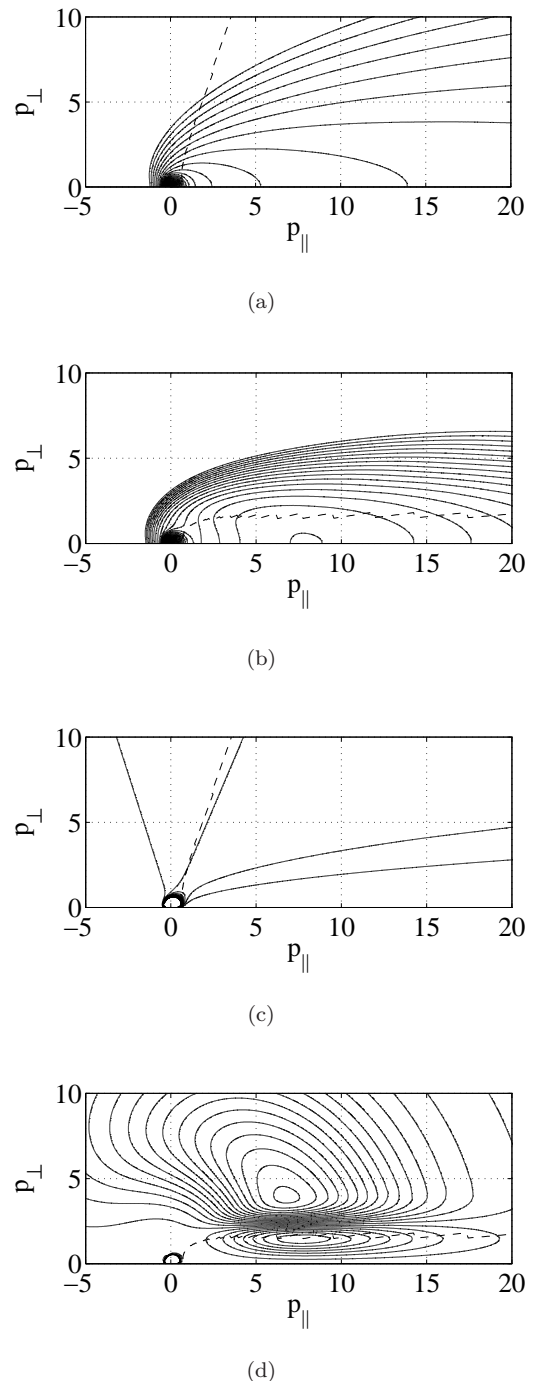


FIG. 2. Contours of the electron distribution function in graphs (a) and (b) and stream function in graphs (c) and (d) in 2-D guiding-center momentum space $(p_{\parallel}, p_{\perp})$ at time $t/\tau_c = 10^6$. The parameters are $E_{\parallel} = 3$, $Z_{\text{eff}} = 1$, $\beta = 0.1$, and $\sigma_r = 0.6$. The ALD force contribution is neglected in (a) and (c) whereas it is accounted for in (b) and (d).

$p_{\perp} < p_{\perp 0}$ at large energies. As seen by the contours of the stream function in Fig 2(d), the steady-state electron flux is directed towards higher energies for $p_{\perp} < p_{\perp 0}$ and towards lower energies for $p_{\perp} > p_{\perp 0}$. The electron tail is thus confined in the region close to $p_{\perp} = 0$, as seen in Fig. 2(b), which creates a strong gradient in p_{\perp} . As seen in the next section, this gradient results in strong pitch-angle scattering, which contributes to limiting the energy of runaway electrons and gives rise to a bump in the distribution under certain conditions. This bump is centered on the p_{\parallel} axis. As the minimum between the bulk and the bump population naturally lies in the vicinity of the critical field, the bump population almost coincides with the runaway region, such that the electron population can be formally separated into a bulk and a runaway “beam”.

B. Perpendicular force balance

The spherical representation (p, ξ) is the natural coordinate system for describing collisions. Thus, it is used for the numerical discretization of the kinetic equation in the Fokker-Planck code LUKE. As seen in Fig. 2(b), however, the tail of the distribution function is determined by the runaway region $p_{\perp} < p_{\perp 0}$ and the natural coordinate system is rather the cylindrical representation $(p_{\perp}, p_{\parallel})$ with $p_{\perp} = p\sqrt{1 - \xi^2}$ and $p_{\parallel} = p\xi$.

The transformation to the $(p_{\perp}, p_{\parallel})$ is detailed in Section A. Focusing on the tail region of momentum space near the parallel axis (characterized by $p_{\perp} \ll p_{\parallel}$ and $p_{\parallel} \gg \beta$), the momentum-space fluxes entering (A2) yield to leading order in β

$$\begin{aligned} S_{\perp} &= -\frac{1 + Z_{\text{eff}}}{2v} \frac{\partial f}{\partial p_{\perp}} - \frac{p_{\perp}}{p_{\parallel}} \left[\frac{1}{v^2} + \sigma_r v (1 + p_{\perp}^2) \right] f, \\ S_{\parallel} &= \left[E_{\parallel} - \frac{1}{v^2} - \sigma_r v p_{\perp}^2 \right] f, \end{aligned} \quad (28)$$

where $v \simeq p_{\parallel}/\gamma \simeq p_{\parallel}/\sqrt{1 + p_{\parallel}^2}$ is the velocity normalized to the speed of light.

At high energy, $v \simeq 1$ and (28) becomes approximately

$$\begin{aligned} S_{\perp} &= -\frac{1 + Z_{\text{eff}}}{2} \frac{\partial f}{\partial p_{\perp}} - \frac{p_{\perp}}{p_{\parallel}} [1 + \sigma_r (1 + p_{\perp}^2)] f, \\ S_{\parallel} &= \sigma_r [p_{\perp 0}^2 - p_{\perp}^2] f. \end{aligned} \quad (29)$$

The parallel flux of electrons S_{\parallel} is positive for particles with $p_{\perp} < p_{\perp 0}$ and negative for particles with $p_{\perp} > p_{\perp 0}$. The resulting strong perpendicular gradient enhances pitch-angle scattering, which creates a positive flux in the p_{\perp} direction at high energy, which is illustrated by the streamlines in Fig. 2(d). This flux limits the extension of the electron distribution to higher energies, as seen in Fig. 2(b). The existence of a bump in the distribution is also driven by the perpendicular dynamics. From the expression (29) for S_{\perp} , we see that the convective component decreases with p_{\parallel} while pitch-angle

scattering is independent of p_{\parallel} for a given perpendicular gradient $\partial f / \partial p_{\perp}$. Therefore, on average, electrons in the tail are pushed into the runaway region at lower p_{\parallel} , while they are scattered away at higher p_{\parallel} . This dynamics is clearly seen in the stream function plot 2(d). Naturally, the bump appears at the balance point where $S_{\perp} \simeq 0$ and electrons accumulate as a result of the perpendicular dynamics. Given the cylindrical symmetry, and since the perpendicular gradient is created by the parallel force balance, we may assume a parabolic dependence scaled by $p_{\perp 0}$ around the bump location

$$\frac{1}{f} \frac{\partial f}{\partial p_{\perp}} \propto -\frac{p_{\perp}}{p_{\perp 0}^2} \quad (30)$$

such that from (29) and for $p_{\perp} \rightarrow 0$ we obtain an estimate for the parametric dependence of the position of the bump

$$p_{\parallel b} \propto \frac{2}{1 + Z_{\text{eff}}} \frac{1 + \sigma_r}{\sigma_r} (E_{\parallel} - 1), \quad (31)$$

which is in agreement with the expression obtained from approximately solving the kinetic equation analytically [15]. It is quite intuitive to expect that the bump energy increases with the electric field amplitude, whereas it decreases with the amplitude of the ALD force and the effective charge. However, the underlying processes are rather complex and involves both the parallel and perpendicular dynamics. The parametric dependence of the bump location predicted by Equation (31) will be compared to numerical calculations in Section V.

C. Validity of the uniform plasma approximation

In tokamak plasmas, particles with purely parallel velocity are subject to an ALD force due to the toroidal and poloidal periodic motions. For a safety factor $q \approx 1$ and electrons with $p_{\parallel} \gg 1$, the contribution from the field line curvature to the ALD force is derived in Appendix C and is expressed as (C3)

$$K_R = -\sigma_r \left(\frac{\rho_0}{R} \right)^2 p_{\parallel}^4, \quad (32)$$

where $\rho_0 = mc/(eB)$ is the Larmor radius of relativistic electrons and R is the major radius. The momentum p_R for which the toroidal ALD and drag forces compensate the electric force is thus given by $E_{\parallel} - 1 - \sigma_r (\rho_0/R)^2 p_R^4 = 0$, which yields

$$p_R = \left(\frac{E_{\parallel} - 1}{\sigma_r} \right)^{1/4} \left(\frac{R}{\rho_0} \right)^{1/2}. \quad (33)$$

For the Tore-Supra example shown in Sec. III, $\rho_0/R = 1.5 \times 10^{-4}$ and we find $p_R = 110$, which corresponds to 55 MeV electrons. We see in Fig. 1(b) that the combination of uniform plasma ALD force and pitch-angle scattering limits the distribution to energies much below 55 MeV. Toroidal effects could thus be neglected in this case.

D. Benchmark of the solution from the LUKE and CODE codes

The simulations presented in this paper were obtained using the code LUKE. While the code is extensively benchmarked for the usual runaway problem [11], LUKE simulations including the ALD reaction force are presented for the first time in this paper. In order to benchmark the numerical simulations, calculations from LUKE are compared to those from the solver CODE, which solves the same Fokker-Planck equation (11) but uses a spectral representation of the pitch-angle dependence [13]. The corresponding steady-state distribution functions are shown in Fig. 3(a) for the parameters used in Sec. III C, and two different values for the effective charge, $Z_{\text{eff}} = 1$ and $Z_{\text{eff}} = 4$. Results from the two codes are in excellent agreement. In particular, both codes show the appearance of a bump at the same energy for $Z_{\text{eff}} = 1$, while they show no bump formation for $Z_{\text{eff}} = 4$.

In addition, the integral part of the collision operator I_{FP} can be included in the code LUKE. Comparing the cases with and without I_{FP} , we find that the distribution functions are very similar, as seen in Fig. 3(b). This is not surprising as I_{FP} mainly affects the bulk population, such that it is appropriate to ignore it in the context of the present paper. However, as I_{FP} ensures momentum conservation in the electron-electron collision operator, it must be included for accurate driven current calculations. Indeed, the current density associated with the distributions shown in Fig. 3(b) is $J/(ecn) = 0.015$ without I_{FP} while it is $J/(ecn) = 0.027$ when I_{FP} is included. The difference arises from a shift of the electron bulk in the parallel direction, which is hardly visible in Fig. 3(b); however, the resulting asymmetry has a strong effect on the corresponding current.

V. PARAMETRIC DEPENDENCES OF THE ELECTRON DISTRIBUTION

The relevant physical parameters for the runaway electron problem described in this paper are the electric field amplitude, the magnitude of the ALD radiation reaction force, the effective charge, and the electron temperature. In this section, the bump formation is characterized as a function of these parameters. The distribution function is evolved until it reaches a steady-state solution.

In a first set of calculations, the electric field is varied while keeping the other relevant parameters fixed, with $Z_{\text{eff}} = 1$, $\beta = 0.1$, and $\sigma_r = 0.6$. The results are shown in Fig. 4. We observe that the electric field must reach a certain threshold for the bump to appear in the tail of the distribution function. Above this threshold, the energy corresponding to the bump location increases with E_{\parallel} , in accordance with the estimate (31). In addition we observe that the number of runaway electrons, i.e. the number of electrons with a positive parallel force balance,

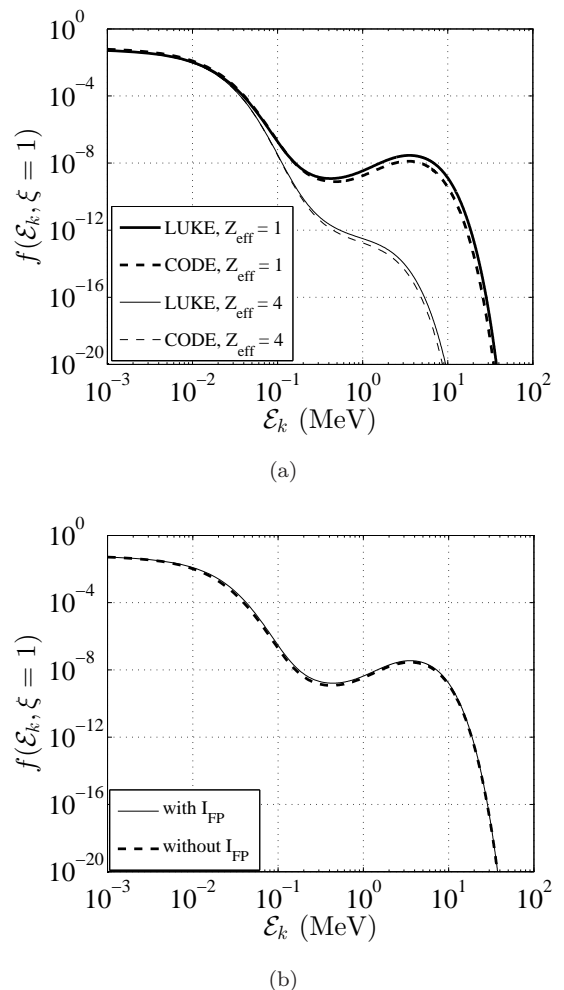
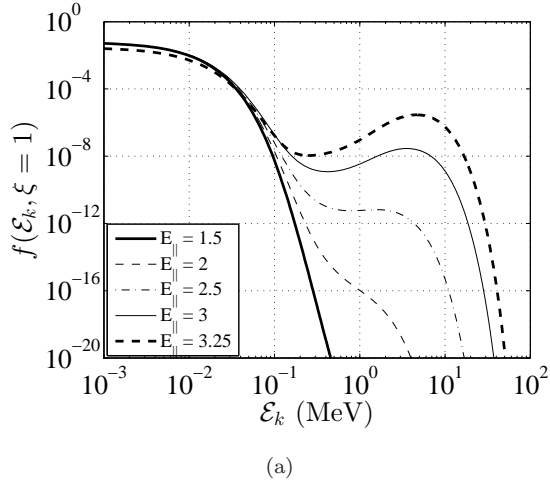


FIG. 3. Electron distribution function in the parallel direction ($\xi = 1$) as a function of the electron kinetic energy ξ_k . Graph (a) compares results from the code LUKE and CODE for $Z_{\text{eff}} = 1$ and $Z_{\text{eff}} = 4$, respectively. Graph (b) compares LUKE calculations in which the integral part of the collision operator I_{FP} is included in the Fokker-Planck equation (9) to the case where it is not. Fixed relevant parameters are $E_{\parallel} = 3$, $\beta = 0.1$, and $\sigma_r = 0.6$.

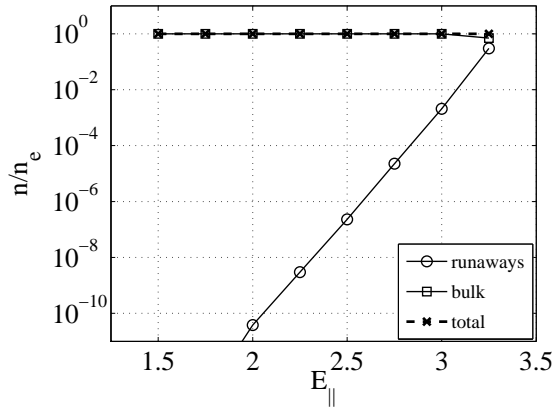
increases with the amplitude of the electric field. Note that the calculation was restricted to $E_{\parallel} < 3.5$, as the linearization of the collision operator fails above this limit since the runaway population becomes of the order of the bulk population.

In a second set of calculations, the electric field is fixed to $E_{\parallel} = 3$, while we vary the amplitude of the synchrotron radiation force, which is proportional to B^2 . The results are shown in Fig. 5. As expected from (31), we observe that the bump size and the location of the bump maximum in energy both decrease if σ_r is increased, to the point where the bump disappears if σ_r is above a certain threshold.

In a third set of calculations, the temperature is varied while the normalized amplitudes of the electric field



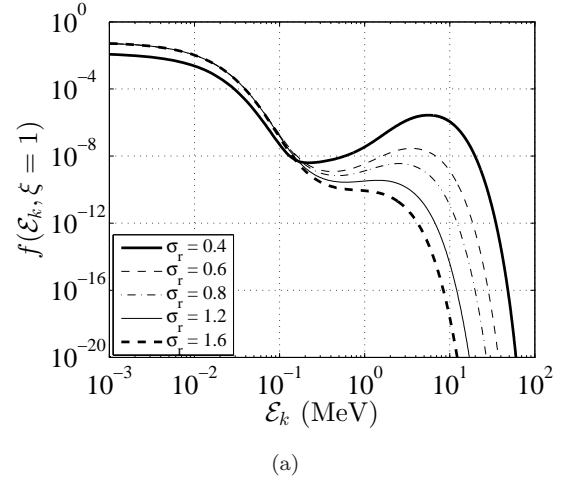
(a)



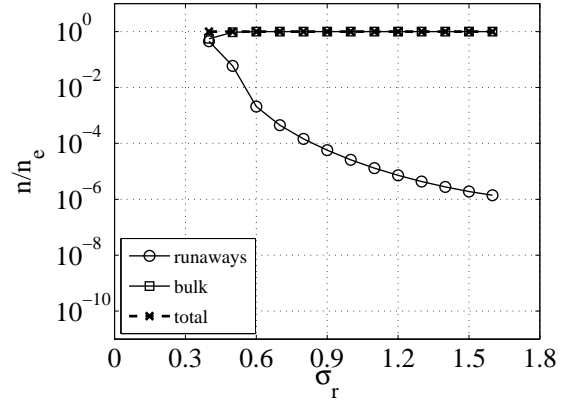
(b)

FIG. 4. (a) Electron distribution function in the parallel direction ($\xi = 1$) as function of the electron kinetic energy \mathcal{E}_k , and (b) fraction of electrons in the runaway region. The simulation results are plotted for various values of the parallel electric field. Fixed relevant parameters are $Z_{\text{eff}} = 1$, $\beta = 0.1$, and $\sigma_r = 0.6$.

and synchrotron radiation force are fixed. The results are shown in Fig. 6. We observe that the bump existence and energy are not affected by the electron bulk temperature, which is again in accordance with the analytical estimate (31). However, the number of electrons in the bump increases strongly with T_e , to the point where the linearization of the collision operator fails for $T_e > 10$ keV with our choice of parameters. This dependence can be explained by the Dreicer effect, which feeds the runaway population from the bulk via collisional diffusion. As seen in Fig. 1(b), the energy corresponding to the minimum between the bulk and the runaway bump decreases with time, until it becomes of the order of the critical energy. At this stage, the minimum coincides with the point where forces balance, such that the collisional diffusion in energy comes to a halt. In other words, the bump population increases until the negative diffusive flux as-



(a)

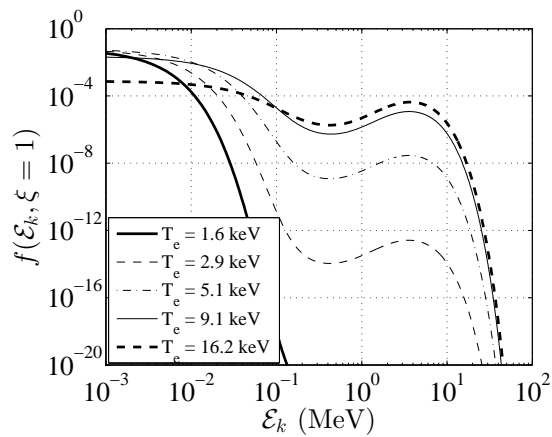


(b)

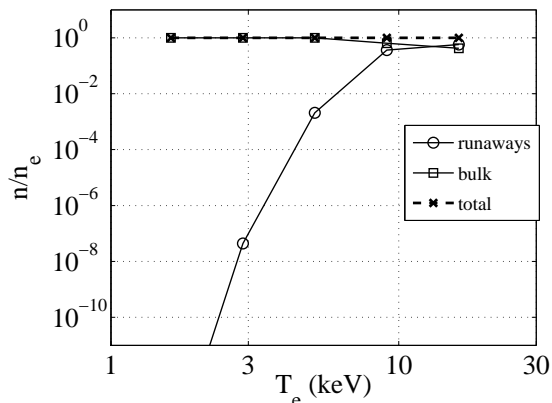
FIG. 5. (a) Electron distribution function in the parallel direction ($\xi = 1$) as a function of the electron kinetic energy \mathcal{E}_k , and (b) fraction of electrons in the runaway region. The simulation results are plotted for various values of the synchrotron reaction force amplitude. Fixed relevant parameters are $Z_{\text{eff}} = 1$, $\beta = 0.1$, and $E_{\parallel} = 3$.

sociated with the positive energy gradient of the bump is sufficient to compensate for the Dreicer flux. Since the latter strongly depends upon the bulk temperature, the bump population evolves accordingly.

Finally, in a fourth set of calculations, the effective ion charge is varied while all other relevant parameters are fixed. The results are shown in Fig. 7. We observe that the bump size and energy decrease with Z_{eff} , to the point where the bump disappears for $Z_{\text{eff}} \geq 3$ with this choice of parameters. The effect of the ion effective charge is predicted by the estimate (31) and understood via the role of pitch-angle scattering, which is proportional to $1 + Z_{\text{eff}}$. For a given perpendicular gradient in the tail of the distribution function - which is determined by the parallel force balance - pitch-angle scattering is the dominant mechanism to extract electrons from the runaway region. The bump can exist only if the perpendicular



(a)



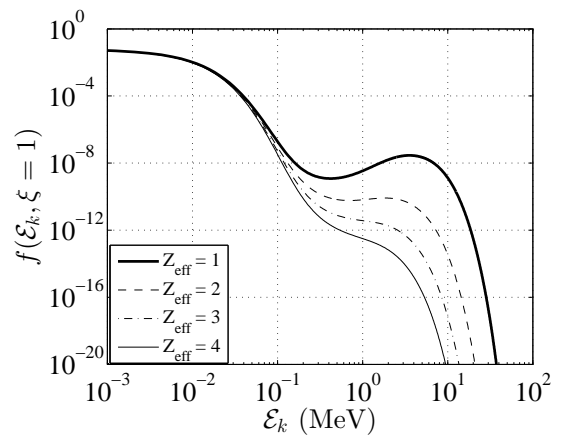
(b)

FIG. 6. (a) Electron distribution function in the parallel direction ($\xi = 1$) as a function of the electron kinetic energy \mathcal{E}_k , and (b) fraction of electrons in the runaway region. The simulation results are plotted for various values of the electron temperature T_e . Fixed relevant parameters are $Z_{\text{eff}} = 1$, $E_{\parallel} = 3$, and $\sigma_r = 0.6$.

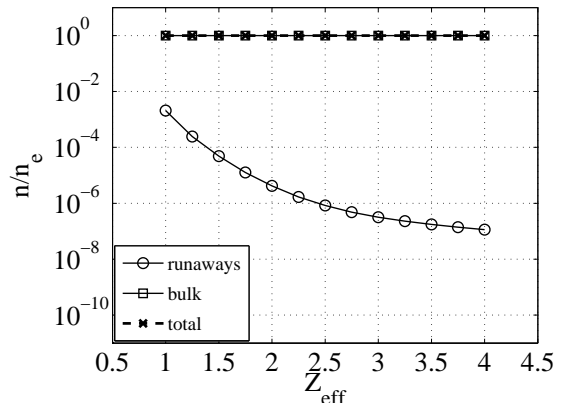
convection due to the synchrotron radiation force and collisional drag dominates over pitch-angle scattering at the lower energies in the runaway region.

VI. CONCLUSIONS

In this paper, the effect of the Abraham-Lorentz-Dirac force in reaction to the synchrotron emission of runaway electrons is investigated for a homogeneous plasma. Whereas a runaway region - with positive force balance - can still be identified in the presence of the ALD force, the electron distribution decreases with momentum at high energy and evolves towards a steady-state solution. This evolution is a result of the strong pitch-angle scattering associated with large gradients in perpendicular momentum. The distribution of electrons is limited to



(a)



(b)

FIG. 7. (a) Electron distribution function in the parallel direction ($\xi = 1$) as a function of the electron kinetic energy \mathcal{E}_k , and (b) fraction of electrons in the runaway region. The simulation results are plotted for various values of the effective charge. Fixed relevant parameters are $\beta = 0.1$, $E_{\parallel} = 3$, and $\sigma_r = 0.6$.

energies well below the value for which the contribution from the toroidal parallel motion to the ALD radiation reaction force becomes significant in a tokamak plasma [9], which justifies the uniform plasma approximation to describe the runaway dynamics in the plasma center.

If the electric force is large compared to the ALD force (proportional to B^2) and the effective charge (which determines the rate of pitch-angle scattering), a bump centered on the parallel momentum axis is formed in the steady-state electron distribution. It results from the competition between the perpendicular convection due to collisions and the ALD force, and pitch-angle scattering. This bump encompasses almost the entire runaway electron population, thus formally dividing the distribution into a bulk population and a runaway beam. The steady-state population of electrons in the bump is found to increase with the bulk electron temperature T_e . The

bump size and average energy increase with the electric field amplitude E_{\parallel} , whereas they decrease with the amplitude of the ALD radiation reaction force and the effective charge.

We can summarize the effect of the ALD radiation reaction force on the electron distribution in three points: first, in accordance with experimental observations it limits the energy gained by runaway electrons to the tens of MeV range; second, it increases the perpendicular anisotropy of the electron distribution, which may give rise to kinetic instabilities such as the EXEL or whistler waves [22–24]; third, it can lead to the formation of a bump in the electron tail, which may give rise to plasma-beam types of kinetic instabilities.

Large amplitude kinetic instabilities generated by the runaway population could pump energy away from electrons and also affect their confinement. Both effects could be beneficial when attempting to limit the threat posed by runaway electrons in tokamaks. Quantifying the effect of kinetic instabilities requires a quasilinear treatment of the kinetic wave-particle interaction, which is beyond the scope of this paper.

More generally, it is interesting to note that any force with a magnitude that increases with the particle energy could play a similar role as the ALD radiation reaction force, resulting in a maximum energy limit for runaways and the possible formation of a bump in the energy distribution.

ACKNOWLEDGMENTS

The work presented in this paper was done while J. D. was invited to work at Chalmers University under the Jubileum professorship award. J. D. would like to express his gratitude to T. Fülöp, the eFT group, and Chalmers University for this opportunity.

Appendix A: Cylindrical representation

The kinetic equation (11) can be expressed in the $(p_{\parallel}, p_{\perp})$ system, which yields

$$\frac{\partial f}{\partial t} + \frac{1}{p_{\perp}} \frac{\partial}{\partial p_{\perp}} (p_{\perp} S_{\perp}) + \frac{\partial}{\partial p_{\parallel}} (S_{\parallel}) = 0, \quad (\text{A1})$$

with the following expressions for the flux components

$$\begin{aligned} S_{\perp} &= -D_{\perp\parallel, \text{FP}} \frac{\partial f}{\partial p_{\parallel}} - D_{\perp\perp, \text{FP}} \frac{\partial f}{\partial p_{\perp}} \\ &\quad + K_{\perp, \text{FP}} f + K_{\perp, \text{E}} f + K_{\perp, \text{ALD}} f, \\ S_{\parallel} &= -D_{\parallel\parallel, \text{FP}} \frac{\partial f}{\partial p_{\parallel}} - D_{\parallel\perp, \text{FP}} \frac{\partial f}{\partial p_{\perp}} \\ &\quad + K_{\parallel, \text{FP}} f + K_{\parallel, \text{E}} f + K_{\parallel, \text{ALD}} f, \end{aligned} \quad (\text{A2})$$

$$\begin{aligned} D_{\perp\perp, \text{FP}} &= \frac{p_{\perp}^2}{p^2} A_{\text{FP}} + \frac{p_{\parallel}^2}{p^2} B_{\text{FP}}, \\ D_{\perp\parallel, \text{FP}} &= \frac{p_{\parallel} p_{\perp}}{p^2} (A_{\text{FP}} - B_{\text{FP}}), \\ D_{\parallel\perp, \text{FP}} &= D_{\perp\parallel, \text{FP}}, \\ D_{\parallel\parallel, \text{FP}} &= \frac{p_{\parallel}^2}{p^2} A_{\text{FP}} + \frac{p_{\perp}^2}{p^2} B_{\text{FP}}, \end{aligned}$$

$$\begin{aligned} K_{\perp, \text{FP}} &= -\frac{p_{\perp}}{p} F_{\text{FP}}, \\ K_{\parallel, \text{FP}} &= -\frac{p_{\parallel}}{p} F_{\text{FP}}, \end{aligned}$$

$$\begin{aligned} K_{\perp, \text{E}}^{\text{C}} &= 0, \\ K_{\parallel, \text{E}}^{\text{C}} &= E_{\parallel}, \end{aligned}$$

$$\begin{aligned} K_{\perp, \text{ALD}}^{\text{C}} &= -\sigma_r \frac{p_{\perp}}{\gamma} (1 + p_{\perp}^2), \\ K_{\parallel, \text{ALD}}^{\text{C}} &= -\sigma_r \frac{p_{\parallel}}{\gamma} p_{\perp}^2. \end{aligned}$$

Appendix B: High-velocity limit

Properties of the electron distribution function are investigated under the conditions that the thermal electron energy is much smaller than the electron rest mass, namely $\beta \ll 1$, and that the electric field is larger than the critical field but much smaller than the Dreicer field $E_D = \beta^{-2}$, meaning

$$1 < E_{\parallel} \ll \beta^{-2} \quad (\text{B1})$$

This ordering implies that runaway electrons are located in the tail of the distribution function, with a momentum $p \gg \beta$ where β is the normalized thermal momentum. For such electrons it is appropriate to take the high velocity limit of the collision operator, which yields

$$A_{\text{FP}}(p) = \frac{\beta^2}{v^3}, \quad (\text{B2})$$

$$F_{\text{FP}}(p) = \frac{1}{v^2}, \quad (\text{B3})$$

$$B_{\text{FP}}(p) = \frac{1 + Z_{\text{eff}}}{2v}. \quad (\text{B4})$$

Appendix C: ALD radiation reaction force for purely parallel motion

In a non-uniform magnetic field, as is found in tokamaks, the field line curvature affects the ALD radiation reaction force. Whereas this effect is expected to be small compared to the contribution from the cyclotron motion for particles with a significant magnetic moment, it could

play a role for particles with $\mathbf{p}_\perp \simeq 0$, for which the contribution from the cyclotron motion (8) vanishes. The combined effects of cyclotron motion and field curvature to the ALD radiation reaction force have been evaluated in a previous work for a purely toroidal magnetic field [9]. Whereas a self-consistent calculation of the ALD radiation reaction force in a tokamak geometry requires a proper guiding-center transformation [20], the importance of the contribution from the field line curvature can be approximately evaluated by considering the motion of a particle with $\mathbf{p}_\perp = 0$. The corresponding guiding center follows the field lines with a velocity $\mathbf{v} = v_\parallel \hat{\mathbf{b}}$, such that the ALD radiation reaction force (7) reduces to

$$\mathbf{K} = \sigma_r \gamma^2 v_\parallel^3 \rho_0^2 \left[\hat{\mathbf{b}} \cdot \nabla \left(\hat{\mathbf{b}} \cdot \nabla \hat{\mathbf{b}} \right) + \gamma^2 v_\parallel \hat{\mathbf{b}} \cdot \left[\hat{\mathbf{b}} \cdot \nabla \left(\hat{\mathbf{b}} \cdot \nabla \hat{\mathbf{b}} \right) \right] \mathbf{v} \right], \quad (\text{C1})$$

where the normalization of Sec. II B is used and with $\rho_0 \equiv mc/(qB)$. In a tokamak with major radius R_0 and circular concentric flux-surfaces characterized by the lo-

cal inverse aspect ratio $\varepsilon = r/R_0 \ll 1$, \mathbf{K} can be expressed as

$$\mathbf{K} = -\sigma_r \gamma \left(\frac{\rho_0}{R_0} \right)^2 p_\parallel^3 \left[\left(1 - v_\parallel^2 \{1 - q^2\} \right) \varepsilon q^{-3} \hat{\boldsymbol{\theta}} + (1 + 2\varepsilon \cos \theta \{q^{-2} - 1\}) \hat{\boldsymbol{\phi}} + \mathcal{O}(\varepsilon^2) \right], \quad (\text{C2})$$

where $\hat{\boldsymbol{\theta}}$ and $\hat{\boldsymbol{\phi}}$ denote the unit vectors in the poloidal and toroidal directions, respectively, θ is the poloidal angle, and $q(\varepsilon)$ is the safety factor. In the case of purely toroidal field lines ($q \rightarrow \infty$) the results from Ref.[9] are retrieved.

The approximation $\varepsilon \ll 1$ is valid near the plasma center, where in addition we typically have $q \simeq 1$, in which case (C2) becomes

$$\mathbf{K} = -\sigma_r \gamma \left(\frac{\rho_0}{R_0} \right)^2 p_\parallel^3 \left[\hat{\mathbf{b}} + \mathcal{O}(\varepsilon^2) \right]. \quad (\text{C3})$$

-
- [1] H. Dreicer. Electron and ion runaway in a fully ionized gas. i. *Phys. Rev.*, 115(2):238–249, 1959.
- [2] T. C. Hender, J.C Wesley, J. Bialek, A. Bondeson, A.H. Boozer, R.J. Buttery, A. Garofalo, T.P Goodman, R.S. Granetz, Y. Gribov, O. Gruber, M. Gryaznevich, G. Giruzzi, S. Günter, N. Hayashi, P. Helander, C.C. Hegna, D.F. Howell, D.A. Humphreys, G.T.A. Huysmans, A.W. Hyatt, A. Isayama, S.C. Jardin, Y. Kawano, A. Kellman, C. Kessel, H.R. Koslowski, R.J. La Haye, E. Lazzaro, Y.Q. Liu, V. Lukash, J. Manickam, S. Medvedev, V. Mertens, S.V. Mirnov, Y. Nakamura, G. Navratil, M. Okabayashi, T. Ozeki, R. Paccagnella, G. Pautasso, F. Porcelli, V.D. Pustovitov, V. Riccardo, M. Sato, O. Sauter, M.J. Schaffer, M. Shimada, P. Sonato, E.J. Strait, M. Sugihara, M. Takechi, A.D. Turnbull, E. Westerhof, D.G. Whyte, R. Yoshino, H. Zohm, the ITPA MHD, Disruption, and Magnetic Control Topical Group. Mhd stability, operational limits and disruptions. *Nucl. Fusion*, 47:S128–S202, 2007.
- [3] V.A. Izzo, E.M. Hollmann, A.N. James, J.H. Yu, D.A. Humphreys, L.L. Lao, P.B. Parks, P.E. Sieck, J.C. Wesley, R.S. Granetz, G.M. Olynik, and D.G. Whyte. Runaway electron confinement modelling for rapid shutdown scenarios in diii-d, alcator c-mod and iter. *Nucl. Fusion*, 51:063032, 2011.
- [4] M. Lehnen, A. Alonso, G. Arnoux, N. Baumgarten, S.A. Bozhentkov, S. Brezinsek, M. Brix, T. Eich, S.N. Gerasimov, A. Huber, S. Jachmich, U. Kruezi, P.D. Morgan, V.V. Plyusnin, C. Reux, V. Riccardo, G. Sergienko, M.F. Stamp, and JET EFDA contributors. Disruption mitigation by massive gas injection in jet. *Nucl. Fusion*, 51(12), 2011.
- [5] R. S. Granetz, B. Esposito, J. H. Kim, R. Koslowski, M. Lehnen, J. R. Martin-Solis, C. Paz-Soldan, T. Rhee, J. C. Wesley, L. Zeng, and ITPA MHD Group. An itpa joint experiment to study runaway electron generation and suppression. *Physics of Plasmas*, 21:072506, 2014.
- [6] E. M. Hollmann, P. B. Aleynikov, T. Fülöp, D. A. Humphreys, V. A. Izzo, M. Lehnen, V. E. Lukash, G. Papp, G. Pautasso, F. Saint-Laurent, and J. A. Snipes. Status of research toward the iter disruption mitigation system. *Phys. Plasmas*, 22:021802, 2015.
- [7] E.M. Hollmann, M.E. Austin, J.A. Boedo, N.H. Brooks, N. Commaux, N.W. Eidietis, D.A. Humphreys, V.A. Izzo, A.N. James, T.C. Jernigan, A. Loarte, J. Martin-Solis, R.A. Moyer, J.M. Muñoz-Burgos, P.B. Parks, D.L. Rudakov, E.J. Strait, C. Tsui, M.A. Van Zeeland, J.C. Wesley, and J.H. Yu. Control and dissipation of runaway electron beams created during rapid shutdown experiments in diii-d. *Nucl. Fusion*, 53(8):083004, 2013.
- [8] W. Pauli. *Theory of Relativity*. Dover Books on Physics. Dover Publications, 1958.
- [9] F. Andersson, P. Helander, and L.-G. Eriksson. Damping of relativistic electron beams by synchrotron radiation. *Phys. Plasmas*, 8(12):5221–5229, 2001.
- [10] A. Stahl, M. Landreman, G. Papp, E. Hollmann, and T. Fülöp. Synchrotron radiation from a runaway electron distribution in tokamaks. *Phys. Plasmas*, 20:093302, 2013.
- [11] J. Decker and Y. Peysson. DKE: A fast numerical solver for the 3D drift kinetic equation. report EUR-CEA-FC-1736, Euratom-CEA, 2004.
- [12] Y. Peysson and J. Decker. Numerical simulations of the radio-frequency driven toroidal current in tokamaks. *Fusion Science and Technology*, 65:22–42, 2014.
- [13] Matt Landreman, Adam Stahl, and Tünde Fülöp. Numerical calculation of the runaway electron distribution function and associated synchrotron emission. *Comp. Phys. Comm.*, 185(3):847 – 855, 2014.
- [14] A. Stahl, E. Hirvijoki, J. Decker, O. Embréus, and T. Fülöp. Effective critical electric field for runaway-electron generation. accepted for publication in *Phys. Rev. Lett.*, 2015.
- [15] E. Hirvijoki, I. Pusztai, J. Decker, O. Embréus, A. Stahl, and T. Fülöp. Radiation reaction induced non-monotonic features in runaway electron distributions. Submitted to *J. Plasma Phys.*, 2015.
- [16] B. J. Braams and C. F. F. Karney. Differential form of

- the collision integral for a relativistic plasma. *Phys. Rev. Lett.*, 59(16):1817–1820, 1987.
- [17] I.P. Shkarofsky and M.M. Shoucri. Modelling of lower hybrid current drive in the presence of spacial radial diffusion. *Nucl. Fusion*, 37(4):539–547, 1997.
 - [18] A.J. Brizard. A guiding-center fokker-planck collision operator for nonuniform magnetic fields. *Phys. Plasmas*, 11(9):4429–4438, 2004.
 - [19] J. Decker, Y. Peysson, A. J. Brizard, and F.-X. Duthoit. Orbit-averaged guiding-center fokker-planck operator for numerical applications. *Phys. Plasmas*, 17(11):112513, 2010.
 - [20] E. Hirvijoki, J. Decker, A. Brizard, and O. Embréus. Guiding-center transformation of the abraham-lorentz-dirac radiation reaction force. submitted to J. Plasma Phys., 2015.
 - [21] C.F.F. Karney. Fokker-planck and quasilinear codes. *Comp. Phys. Rep.*, 4:183–244, 1986.
 - [22] G.I. Pokol, T. Fülöp, and M. Lisak. Quasi-linear analysis of whistler waves driven by relativistic runaway beams in tokamaks. *Plasma Phys. Control. Fusion*, 50:045003, 2008.
 - [23] A. Kómár, G.I. Pokol, and T. Fülöp. Electromagnetic waves destabilized by runaway electrons in near-critical electric fields. *Phys. Plasmas*, 20:012117, 2013.
 - [24] G.I. Pokol, A. Kómár, A. Budai, A. Stahl, and T. Fülöp. Quasi-linear analysis of the extraordinary electron wave destabilized by runaway electrons. *Phys. Plasmas*, 21:102503, 2014.